BIOCHEMISTRY
including biophysical chemistry & molecular biology

Article

pubs.acs.org/biochemistry

Solution Structure of Kurtoxin: A Gating Modifier Selective for Cav3 Voltage-Gated Ca^{2+} Channels

Chul Won Lee,[†,‡] Chanhyung Bae,[†] Jaeho Lee,[†] Jae Ha Ryu,[†] Ha Hyung Kim,[§] Toshiyuki Kohno,[∥] Kenton J. Swartz,[⊥] and Jae Il Kim*[,†]

[†]Department of Life Science, Gwangju Institute of Science and Technology (GIST), Gwangju 500-712, Republic of Korea

[‡]Department of Chemistry, Chonnam National University, Gwangju 500-757, Republic of Korea

[§]College of Pharmacy, Chung-Ang University, Seoul 156-756, Republic of Korea

[∥]Department of Biochemistry, Kitasato University, School of Medicine, Kanagawa 252-0374, Japan

[⊥]Molecular Physiology and Biophysics Section, National Institute of Neurological Disorders and Stroke, National Institutes of Health, Bethesda, Maryland 20892, United States

Supporting Information

ABSTRACT: Kurtoxin is a 63-amino acid polypeptide isolated from the venom of the South African scorpion *Parabuthus transvaalicus*. It is the first and only peptide ligand known to interact with Cav3 (T-type) voltage-gated Ca^{2+} channels with high affinity and to modify the voltage-dependent gating of these channels. Here we describe the nuclear magnetic resonance (NMR) solution structure of kurtoxin determined using two- and three-dimensional NMR spectroscopy with dynamical simulated annealing calculations. The molecular structure of the toxin was highly similar to those of scorpion α-toxins and contained an α-helix, three β-strands, and several turns stabilized by four disulfide bonds. This so-called "cysteine-stabilized α-helix and β-sheet (CS$\alpha\beta$)" motif is found in a number of functionally varied small proteins. A detailed comparison of the backbone structure of kurtoxin with those of the scorpion α-toxins revealed that three regions [first long loop (Asp[8]–Ile[15]), β-hairpin loop (Gly[39]–Leu[42]), and C-terminal segment (Arg[57]–Ala[63])] in kurtoxin significantly differ from the corresponding regions in scorpion α-toxins, suggesting that these regions may be important for interacting with Cav3 (T-type) Ca^{2+} channels. In addition, the surface profile of kurtoxin shows a larger and more focused electropositive patch along with a larger hydrophobic surface compared to those seen on scorpion α-toxins. These distinct surface properties of kurtoxin could explain its binding to Cav3 (T-type) voltage-gated Ca^{2+} channels.

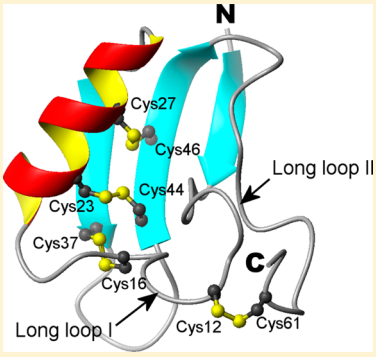

Voltage-gated ion channels are expressed by nearly all cells and play a crucial role in regulating membrane potential and a variety of cellular functions. These channels are comprised of two principle domains: a central pore domain formed by two segments, S5 and S6, and four surrounding voltage-sensing domains, each composed of segments S1–S4.[1−4] Venomous animals (spiders, scorpions, and cone snails, among others) produce a broad array of polypeptide toxins, many of which bind to voltage-gated Na^+, K^+, or Ca^{2+} channels,[5−8] and have proven to be valuable pharmacological tools for evaluating specific channel characteristics.

Although the origins of the venomous peptide toxins that interact with voltage-gated ion channels are diverse, their modes of action fall into two major categories, pore blockade and gating modification, based on the domain with which they interact and their mechanisms of action. Pore blockers bind to the external vestibule of the channel and physically obstruct the movement of ions by occluding the ion-conducting pore.[9] The three-dimensional structures of many pore-blocking toxins, including the μ-conotoxins for the Na^+ channel, charybdotoxin for the K^+ channel, and ω-conotoxins for the Ca^{2+} channel, have all been determined, allowing investigation of the structure–function relationships of the pore-forming domains of the channels.[10−15] Gating modifiers, on the other hand, bind to the voltage-sensing domains of voltage-gated ion channels and modify the energetics of either activation or inactivation.[16−21] Established gating modifiers include the α- and β-scorpion toxins, sea anemone toxins, and δ-conotoxins for Na^+ channels;[22−28] hanatoxin (HaTx), SGTx1, GxTx-1E, and VSTx for K^+ channels;[29−33] and ω-agatoxin IVA (ω-Aga IVA) and ω-grammotoxin SIA (GrTx) for Ca^{2+} channels.[34−37]

Studies of the structure and function of gating modifiers have advanced our understanding of the molecular structures and gating mechanisms of voltage-gated ion channels. Studies employing HaTx, SGTx1, GxTx-1E, VSTx, GrTx, and ω-Aga IVA have revealed that, within voltage-gated K^+ and Ca^{2+} channels, these proteins bind to structurally conserved motifs composed of hydrophobic and acidic residues within the C-

Received: October 27, 2011
Revised: February 13, 2012
Published: February 13, 2012

 © 2012 American Chemical Society

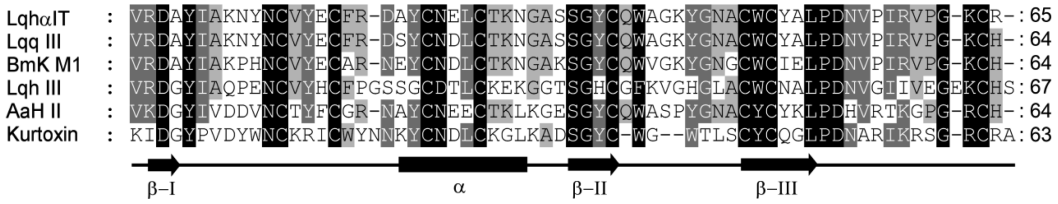

Figure 1. Amino acid sequences and alignment of kurtoxin and five scorpion α-toxins. LqhαIT and Lqq III are highly active in insects. Lqh III and Bmk M1 are α-like toxins. AaH II is highly active in mammals. These sequences were aligned using ClustalX. Highly conserved residues are shaded in black or gray. The secondary structure elements of kurtoxin are shown as arrows (β-strand), bars (α-helix), and lines (connecting loops).

terminal end of S3 and the N-terminal end of S4.[17−19,38−42] The X-ray structures of voltage-gated K^+ channels (i.e., KvAP and Kv1.2 channels) show that these regions of S3 and S4 form a helix−turn−helix motif termed the voltage sensor paddle.[4,43,44] Gating modifier toxins that partition into the membrane interact with the voltage sensor paddle at the protein−lipid interface.[42,45]

Cav3 (T-type) voltage-gated Ca^{2+} channels can be differentiated from other types of Ca^{2+} channels on the basis of their activation at lower voltages, faster inactivation, slower deactivation, and smaller Ba^{2+} conductances.[46] Their unique gating properties allow Cav3 (T-type) Ca^{2+} channels to trigger low-threshold spikes that can lead to burst firing and oscillatory behavior and can contribute to standing calcium currents near the resting membrane potential in a variety of cell types.[47−50] Although these characteristics imply Cav3 (T-type) channels could play important roles in many tissues,[51,52] progress in understanding their subunit composition and physiological functions has been hindered by a scarcity of ligands that interact with these channels.[53,54]

A gating modifier kurtoxin, isolated from the venom of the scorpion *Parabuthus transvaalicus*, is the first peptide ligand known to act on Cav3 (T-type) voltage-gated Ca^{2+} channels.[55,56] Here, we describe the solution structure of kurtoxin determined using proton two-dimensional (2D) and heteronuclear three-dimensional (3D) NMR spectroscopy with dynamical simulated annealing calculations. The structure of kurtoxin closely resembles those of scorpion α-toxins (Figure 1) targeting Na^+ channels and shows the unique structural characteristic of gating modifiers, electropositive and hydrophobic patches on the surface of the molecule.[39,57,58] Detailed inspection of the structure of kurtoxin offers the possibility of understanding the molecular basis of its Cav3 (T-type) Ca^{2+} channel selectivity and could facilitate clarification of the gating mechanism of voltage-gated ion channels.

EXPERIMENTAL PROCEDURES

Sample Preparation. Functional kurtoxin was obtained using a bacterial expression system.[59] The recombinant kurtoxin was expressed as an inclusion body, solubilized in a denaturing solution, and then refolded in a refolding solution. The crude folded kurtoxin was purified by preparative RP-HPLC, after which the purity of the recombinant protein was confirmed by analytical RP-HPLC and MALDI-TOF MS measurements.

CD Spectral Analysis. CD spectra were recorded on a JASCO J-750 spectropolarimeter in a solution containing 0.01 M sodium phosphate in H_2O and 0, 10, 15, 20, 25, or 30% CH_3CN at pH 7.0. Measurements were taken at 20 °C using a quartz cell with a 1 mm path length. The spectra were expressed as molecular ellipticity $[\theta]$ in degrees square centimeter per decimole.

NMR Spectroscopy. NMR measurements were taken on a Bruker AVANCE 600 spectrometer equipped with an xyz gradient triple-resonance probe. The samples used for proton 2D NMR experiments were 1 mM kurtoxin dissolved in water containing 25% CD_3CN at pH 4.0 (uncorrected for the isotope effect). All proton 2D NMR spectra were recorded in a phase-sensitive mode using time-proportional phase incrementation (TPPI) for quadrature detection in the t_1 dimension at 278, 288, and 298 K. TOCSY spectra were recorded using a MLEV-17 pulse scheme[60] with isotropic mixing times of 60 and 90 ms. NOESY spectra[60−62] were recorded with mixing times of 60, 100, and 150 ms. Suppression of the solvent resonance in both the NOESY and TOCSY measurements was achieved using the WATERGATE scheme.[63] E-COSY[64] spectra were recorded to obtain the constraints for stereospecific assignments.

The following triple-resonance 3D NMR spectra were recorded using 1 mM ^{13}C- and ^{15}N-labeled or 1 mM ^{15}N-labeled kurtoxin in 25% CD_3CN at 278 and 288 K. Uniformly ^{13}C- and ^{15}N-enriched kurtoxin was used to record 3D HNCACB, CBCA(CO)NH, HNCA, HN(CO)CA, HNCO, and HN(CA)CO spectra.[65−68] Uniformly ^{15}N-enriched kurtoxin was used to record 2D $^1H-^{15}N$ HSQC[69] and 3D ^{15}N TOCSY-HSQC spectra with 90 ms mixing times and a 3D ^{15}N NOESY-HSQC spectrum with a 120 ms mixing time. The $^3J_{HN-H^\alpha}$ values were obtained from the 3D HNHA[70] and 2D DQF-COSY spectra. Slowly exchanging backbone amide protons were identified by analysis of TOCSY spectra recorded in 75% D_2O and 25% CD_3CN on time scales of 30 min and 3.5 h and then every 3 h up to 25 h. ^1H chemical shifts were referenced to DSS at 0 ppm, and ^{13}C and ^{15}N chemical shifts were calculated from the ^1H frequency. All spectra were processed using AZARA version 2.5 (provided by W. Boucher) or XWIN-NMR and were analyzed using ANSIG version 3.3[71] on a Silicon Graphics Octane2 workstation or on a Linux workstation.

NMR Experimental Restraints and Structure Calculations. The backbone $NH-C^\alpha H$ coupling constants were converted to backbone torsion angle ϕ constraints according to the following rules: for a $^3J_{NH-C^\alpha H}$ of <5.5 Hz, the ϕ angle was constrained in the range of $-65 \pm 25°$; for a $^3J_{NH-C^\alpha H}$ of >8.0 Hz, it was constrained in the range of $-120 \pm 40°$.[72,73] Backbone dihedral constraints were not applied to $^3J_{NH-C^\alpha H}$ values between 5.5 and 8.0 Hz. The range of the χ^1 side chain torsion angle constraints and the stereospecific assignment of the prochiral β-methylene protons were obtained using the $^3J_{\alpha\beta}$ coupling constants combined with the intraresidue $NH-C^\beta H$ NOEs.[74] The $^3J_{\alpha\beta}$ coupling constants were determined from the E-COSY spectrum in D_2O. For the t^2g^3, g^2g^3, and g^2t^3 conformations around the $C^\alpha-C^\beta$ bonds, the χ^1 side chain

dx.doi.org/10.1021/bi201633j | *Biochemistry* 2012, 51, 1862−1873

torsion angle was constrained in the ranges of −60 ± 30°, 60 ± 30°, and 180 ± 30°, respectively.[75]

Quantitative determination of the cross-peak intensities was based on the counting levels. Observed NOE data were classified into four distance ranges (1.8−2.7, 1.8−3.5, 1.8−5.0, and 1.8−6.0 Å) that corresponded to strong, medium, weak, and very weak NOE values, respectively. Pseudoatoms were used for the methyl protons or the nonstereospecifically assigned methylene protons.[76] Correcting factors for the use of pseudoatoms were added to the distance constraints, and 0.5 Å was added to the distance constraints involving methyl protons.[77] For each disulfide bond, we used three distance constraints, $S(i)-S(j)$, $S(i)-C^{\beta}(j)$, and $S(j)-C^{\beta}(i)$, whose target values were set to 2.02 ± 0.02, 2.99 ± 0.5, and 2.99 ± 0.5 Å, respectively.[78] The hydrogen bond acceptors for the slowly exchanged amide protons were identified by analyzing the preliminarily calculated structures.[79,80] The distance restraints on the hydrogen bonds were added as target values of 1.8−2.3 Å for $NH(i)-O(j)$ and 2.8−3.3 Å for $N(i)-O(j)$ bonds.

All calculations were conducted on an SGI Octane2 workstation using the X-PLOR version 3.851.[81] The three-dimensional structures were calculated on the basis of the experimentally derived distance and torsion angle constraints using a dynamically simulated annealing protocol starting from a template structure with randomized backbone ϕ and ψ torsion angles. The final 20 structures with the lowest energy and smallest Lennard-Jones van der Waals energy were chosen. The convergence of the calculated structures was evaluated in terms of the structural parameters. There were root-mean-square deviations (rmsds) from the experimental distances and dihedral constraints, from the energetic statistics (E_{NOE}, E_{tor}, E_{repel}, and $E_{L\text{-}J}$), and from the idealized geometry. The structures were analyzed using the PROCHECK_NMR,[82] PROMOTIF,[83] MOLMOL,[84] and MolProbity.[85,86] The distributions of the backbone dihedral angles in the final converged structure were evaluated by representation of the Ramachandran dihedral pattern, which indicated the deviations from the allowed ϕ and ψ angle limits. The degrees of angular variation among the converged structures were further assessed using an angular order parameter.[87] The solvent-accessible surface areas for the side chains of the amino acid residues were calculated with a solvent radius of 1.4 Å. Structural figures were generated using MOLMOL and INSIGHT II 2000 (Accelrys Inc.).

RESULTS AND DISCUSSION

NMR Sample Preparation. Kurtoxin was insoluble in aqueous solution, even at a concentration of <1 mM. We therefore tested whether kurtoxin could be solubilized using 0−30% acetonitrile (CH_3CN) without disrupting the protein's intrinsic structure. Figure 2 shows that the CD spectra for kurtoxin recorded in the absence or presence of 10, 15, 20, 25, and 30% CH_3CN are nearly identical in the far-UV region (200−250 nm), indicating that the backbone structure of kurtoxin is affected little by the addition of CH_3CN. Moreover, we obtained high-quality NMR spectra with 1 mM kurtoxin in the presence of 25% deuterated acetonitrile (CD_3CN), strongly suggesting that the addition of CD_3CN effectively prevented the aggregation of kurtoxin (Figure 3). In the $^1H-^{15}N$ HSQC spectra recorded in pure water, several hydrophobic peaks, including Tyr^{17}, Tyr^{18}, Trp^{38}, Gly^{39}, Trp^{40}, and Leu^{42}, could not be detected, most likely because of the line broadening in the absence of CD_3CN (Figure 3). This appeared to be due to the

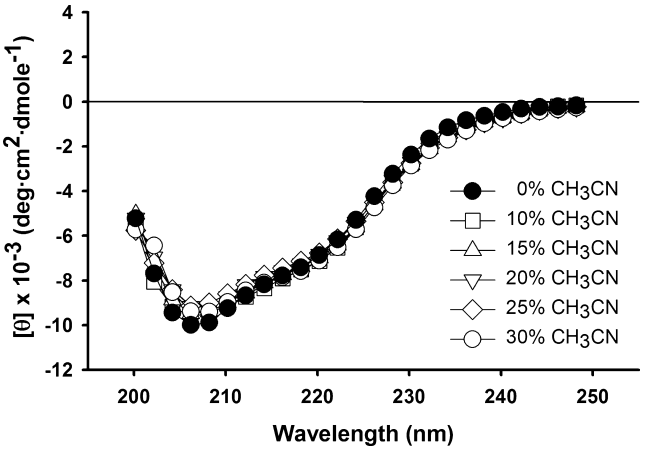

Figure 2. CD spectra of 0.05 mM kurtoxin in H_2O containing 0, 10, 15, 20, 25, or 30% CH_3CN [0.01 M sodium phosphate (pH 7.0)] at 20 °C.

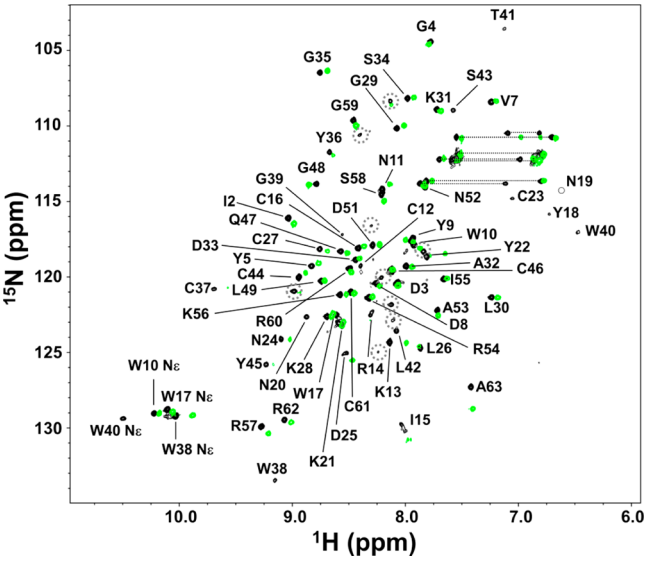

Figure 3. $^1H-^{15}N$ HSQC spectra of kurtoxin in the presence (black) and absence (green) of 25% CD_3CN at 288 K. The resonance assignments are indicated by the one-letter amino acid codes and residue numbers. The dotted circles indicate additional and unassigned peaks.

self-aggregation of kurtoxin molecules. On the other hand, in the $^1H-^{15}N$ HSQC spectra recorded in the presence of 25% CD_3CN, all of the backbone $^1H-^{15}N$ cross peaks were identifiable, and the intensities of nearly all the peaks were increased without large chemical shift variations (Figure S1 of the Supporting Information).

Addition of CH_3CN can weaken the hydrophobic interactions between surface hydrophobic regions without altering the three-dimensional structure of the proteins.[88] Nonetheless, CH_3CN can influence chemical shift variations by changing the polarity of the accessible atom environments; of those, the chemical shifts located in the flexible N- and C-terminal regions (Ala^{63} of kurtoxin in Figure S1 of the Supporting Information) and loops are most sensitive.[89] Comparison of the CD and $^1H-^{15}N$ HSQC spectra recorded in the presence and absence of 25% CD_3CN indicates that CD_3CN prevented the hydrophobic-related aggregation of kurtoxin without disrupting its overall topology. Linear kurtoxin

dx.doi.org/10.1021/bi201633j | Biochemistry 2012, 51, 1862−1873

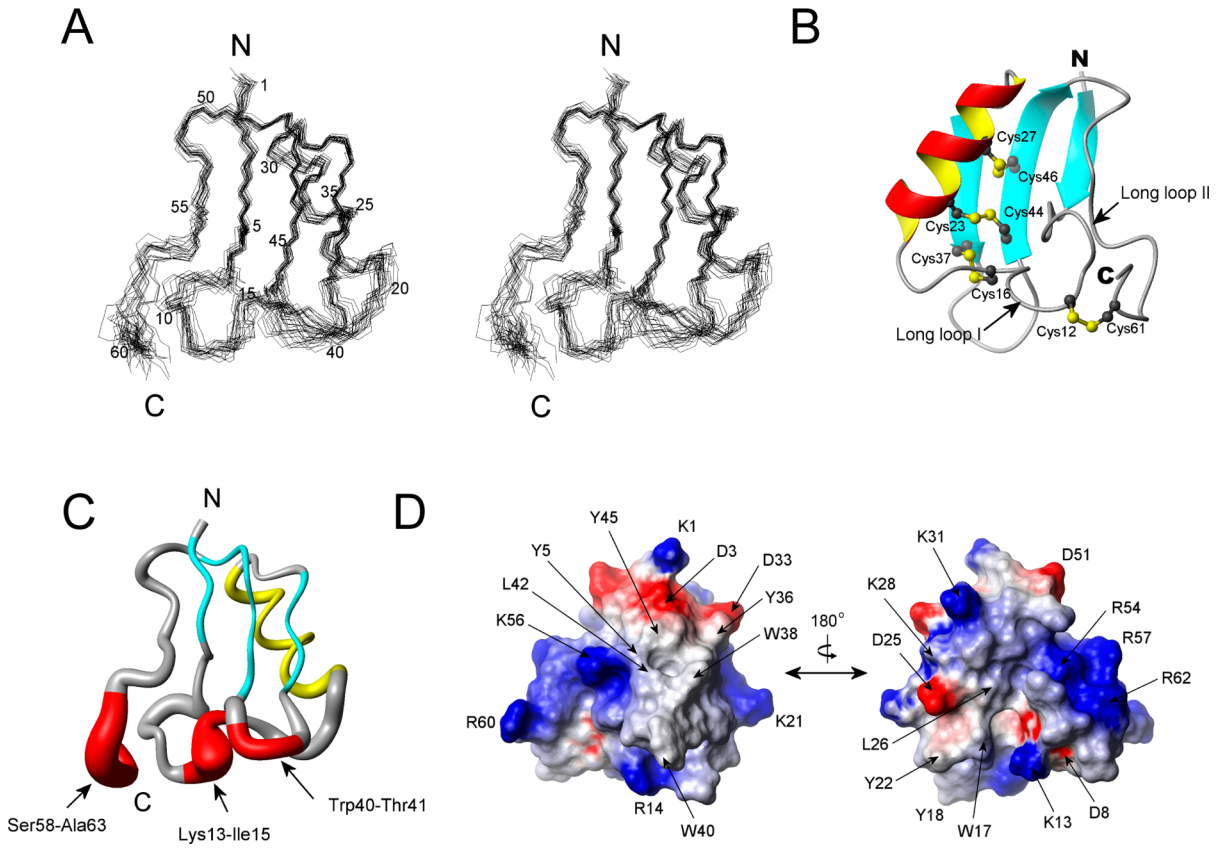

Figure 4. Solution structure of kurtoxin. (A) Stereopairs of backbone heavy atoms (N, C^{α}, and C) for the 20 converged structures of kurtoxin. These are the results of the best-fit superposition of the backbone heavy atoms of the molecule. N and C indicate N- and C-terminal positions, respectively. (B) Ribbon structure of kurtoxin. Schematic diagram of kurtoxin illustrating the location of the β-strands (cyan), α-helix (red and yellow), and disulfide bonds (numbered ball and stick). Long loop I and long loop II correspond to residues Tyr^{5}–Asn^{20} and Pro^{50}–Ala^{63}, respectively. (C) Tubular representation of kurtoxin illustrating its motional properties. The diameter of the tube is proportional to the atomic rmsds of the backbone atoms: red for residues whose backbone rmsds are >1.0, cyan for those with β-strands, and yellow for those with an α-helix. (D) Surface profile of kurtoxin. The surface hydrophobic patches and charged residues are indicated. The molecular surface of kurtoxin is shown in color according to the electrostatic potential: red for negatively charged amino acids, blue for positively charged amino acids, and white for uncharged or hydrophobic amino acids. The left and right figures are rotated 180° with respect to one another about a vertical axis. These figures were generated using MOLMOL.

was also refolded in a redox solution containing 30% CH_3CN,[59] suggesting the nativelike conformation of kurtoxin is stabilized in an aqueous solution containing CH_3CN.

A small number of additional minor peaks were observed in NMR spectra, including ^{1}H–^{15}N HSQC spectra in the presence and absence of CD_3CN (Figure 3). The intensity ratio of the minor peaks is <5–10% compared to that of the major peaks according to relevant NMR signals. Unfortunately, we failed to assign these minor peaks because the signals were very weak and it was hard to sequentially connect these minor peaks. In a recent study, two stable conformations of Bm$\kappa\alpha$Tx11, a kurtoxin-homologous scorpion α-toxin, were identified by using NMR spectroscopy.[90] We assume that the minor peaks of kurtoxin also come from a possible minor conformation similar to Bm$\kappa\alpha$Tx11.

NMR Spectroscopy. Sequence-specific assignments for the backbone atoms of kurtoxin were obtained from an analysis of heteronuclear 3D NMR spectra [HNCACB, CBCA(CO)-NNH, HNCA, and HN(CO)CA] recorded in 25% CD_3CN at pH 4.0 and 288 and 278 K using a uniformly ^{15}N- and ^{13}C-labeled protein. All backbone C^{α} atoms were assigned except those of Cys^{12}, Arg^{14}, Ile^{15}, Asp^{25}, Leu^{26}, Ala^{32}, and Trp^{40}. The backbone and side chain protons were obtained from 2D NMR spectra (DQF-COSY, TOCSY, and NOESY) and 3D ^{15}N NOESY-HSQC and 3D ^{15}N TOCSY-HSQC spectra recorded in 25% CD_3CN at pH 4.0 and 288 K. The assignments of all backbone and side chain protons were complete except for those of the H^{ζ} atoms of Lys^{13} and Lys^{21}, $H^{\delta 2}$ of Asn^{19} and Asn^{20}, and H^{δ} and H^{ϵ} of Tyr^{22}. For all Pro residues (Pro^{6} and Pro^{50}), strong sequential $d_{\alpha,\delta}$ and no $d_{\alpha,\alpha}$ were observed in the NOESY spectra, indicating the toxin's proline residues are all in the *trans* configuration.

Identification of Secondary Structure Elements. As summarized in Figure S2 of the Supporting Information, the pattern of observed NOEs and chemical shift index (CSI) values for H^{α} was ultimately interpreted in terms of the secondary structure of the molecule. The weak $^{3}J_{HN^{\alpha}}$ coupling constants, strong d_{NN} NOE peaks and $d_{\alpha N}(i,i+3)$ and $d_{\alpha\beta}(i,i+3)$ NOE correlations, and the CSI value of −1 all indicate an α-helical conformation for residues Lys^{21}–Leu^{30}. The extent of the β-strands and their relative orientations within the β-sheet structure were determined using standard criteria: large $^{3}J_{HN^{\alpha}}$ coupling constants (Ile^{2}, Asp^{3}, Try^{36}, Cys^{37}, Tyr^{45}, Cys^{46}, and Gln^{47}), strong sequential $d_{\alpha N}$, interstrand NH–NH and NH–$C^{\alpha}H$ connectivities, and slowly exchanging amide protons (Ile^{2}, Gly^{4}, Gly^{35}, Tyr^{36}, Cys^{44}, Tyr^{45}, Cys^{46}, Gln^{47}, and Leu^{49}).

dx.doi.org/10.1021/bi201633j | *Biochemistry* 2012, 51, 1862–1873

Kurtoxin contains three β-strands comprised of residues Ile^2–Gly^4, Ser^{34}–Cys^{37}, and Cys^{44}–Leu^{49}, which are arranged in an antiparallel fashion with several turns (Figure S3 of the Supporting Information). Our criteria allowed discrimination of the peripheral and central strands within the β-sheet.

Structure Calculations. The structure of kurtoxin was determined from a total of 894 NMR experimental constraints, including 856 experimental distance constraints and 38 dihedral angle constraints, which correspond to an average of 14.2 constraints per residue. Of the 861 distance constraints, there were 311 intraresidue and 492 interresidue NOE distance constraints, 42 hydrogen bond constraints determined from hydrogen–deuterium exchange-out experiments, and 12 disulfide bond constraints. The 42 distance constraints related to hydrogen bonds were as follows: I2(HN)–L49(CO), G4(HN)–C46(CO), D25(HN)–K21(CO), C27(HN)–C23(CO), K28(HN)–N24(CO), G29(HN)–L26(CO), L30(HN)–C27(CO), K31(HN)–K28(CO), A32(HN)–C27(CO), G35(HN)–D33(CO), Y36(HN)–Y45(CO), W38(HN)–S43(CO), C44(HN)–I15(CO), Y45(HN)–Y36(CO), C46(HN)–G4(CO), Q47(HN)–S34(CO), L49(HN)–I2(CO), A53(HN)–P50(CO), K56(HN)–Y5(CO), R62(HN)–W10(CO), and A63(HN)–C61(CO). The disulfide bond pattern of kurtoxin was determined to be Cys^{12}–Cys^{61}, Cys^{16}–Cys^{37}, Cys^{23}–Cys^{44}, and Cys^{27}–Cys^{46}, based on sequential cleavage with proteases and MALDI-TOF MS measurements.[59]

We conducted the simulated annealing calculations starting with 100 random kurtoxin structures. From those, we selected 20 final structures (Figure 4A) that were in good agreement with the NMR experimental constraints (NOE distance and torsion angle violations of <0.2 Å and <2°, respectively). Statistics for the converged structures were evaluated in terms of the structural parameters (Table 1). The deviations from the idealized covalent geometry were very small, and the Lennard-Jones van der Waals energy was large and negative (−212.55 ± 19.40), indicating there were no distortions or nonbonded bad contacts in the converged structures. The atomic rmsd about the mean coordinate positions was 0.87 ± 0.14 Å for the backbone atoms (N, C$^\alpha$, and C) and 1.54 ± 0.19 Å for all heavy atoms. Ramachandran analysis showed that 98.7% of all residues fell within allowed regions.

Structure Description. The molecular structure of kurtoxin has a compact core consisting of an α-helix and a triple-stranded antiparallel β-sheet stabilized by four disulfide bridges. The 2.5-turn α-helix is composed of residues extending from Lys^{21} to Leu^{30} and is linked to the central strand of the β-sheet by two disulfide bridges (Cys^{23}–Cys^{44} and Cys^{27}–Cys^{46}) (Figure 4B). The three β-strands are formed by residues Ile^2–Gly^4 (β-strand I), Ser^{34}–Cys^{37} (β-strand II), and Cys^{44}–Leu^{49} (β-strand III), with residues Ile^2, Gly^{48}, and Leu^{49} involved in a β-bulge conformation. The last two residues of β-strand III (Gly^{48} and Leu^{49}) form a classical β-bulge and interact with the first residue of β-strand I (Ile^2). As a result, the ϕ angle of Gly^{48} is positive (105.6°), which causes a distortion in the β-sheet. Two long loops (loop I, Tyr^5–Asn^{20}; loop II, Pro^{50}–Ala^{63}) extend from the core (Figure 4B). Long loop I includes two type IV β-turns (Asp^8–Asn^{11} and Asn^{11}–Arg^{14}) and adopts the positive ϕ angles (58.9° and 89.9°, respectively) of Asn^{11} and Arg^{14} in the average structure. Long loop I is connected to β-strand II by a disulfide bond (Cys^{16}–Cys^{37}) and to the C-terminus by a disulfide bond (Cys^{12}–Cys^{61}) and a hydrogen bond [R62(HN)–W10(CO)]. Long loop II starts with a well-defined type I β-turn structure (residues 50–53) and extends to the C-terminus. It is stabilized through hydrogen bonding [N11(HD21)–S58(CO), K56(HN)–Y5(CO), and R62(HN)–W10(CO)] and formation of a disulfide bridge (Cys^{12}–Cys^{61}) to long loop I. The short loop regions (Lys^{13}–Ile^{15} and Trp^{40}–Thr^{41}) and the six C-terminal residues (Ser^{58}–Ala^{63}) are less defined in the final 20 structures than the other regions in kurtoxin (Figure 4C). This may reflect a lack of medium- and long-range NOE constraints due to the inherent flexibility of these regions.

Two surface hydrophobic patches were observed in the kurtoxin structure. The major patch is composed of the solvent-exposed side chains of Tyr^5, Tyr^{36}, Trp^{38}, Trp^{40}, Leu^{42}, and Tyr^{45} (Figure 4D), which, except for Tyr^5, are located in the hairpin structure (strands II and III). Their side chains are well stacked, creating a compact hydrophobic patch on the surface of the molecule. The minor hydrophobic patch is situated on the opposite side of the protein and is centered around Trp^{17}, Tyr^{18}, Tyr^{22}, and Leu^{26} (Figure 4D). Interestingly, all line-broadened residues (including Tyr^{17}, Tyr^{18}, Trp^{38}, Gly^{39}, Trp^{40}, and Leu^{42}) in pure water are located within either the major or minor surface hydrophobic patch in kurtoxin, strongly suggesting that the aggregation of kurtoxin results from these hydrophobic surface properties of kurtoxin. All of the charged residues except Asp^8 are highly exposed on the surface of

Table 1. Structural Statistics for the 20 Lowest-Energy Structures of Kurtoxin[a]

rmsd from experimental distance constraints (Å)[b] (856)	0.0115 ± 0.0012
rmsd fom experimental dihedral constraints (deg)[b] (38)	0.1555 ± 0.0012
energetic statistics (kcal/mol)[c]	
F_{NOE}	5.7261 ± 1.2582
F_{tor}	0.9845 ± 0.0964
F_{repel}	5.3839 ± 1.3992
$E_{L\text{-}J}$	−212.55 ± 19.4000
rmsd from idealized geometry	
bonds (Å)	0.0017 ± 0.0001
angles (deg)	0.5010 ± 0.0065
impropers (deg)	0.3391 ± 0.0060
Ramachandran analysis[d] (%)	
most favored regions	56.0
additionally allowed regions	36.1
generously allowed regions	6.5
disallowed regions	1.3
average rmsd (Å)	
backbone (N, C$^\alpha$, C)	0.87 ± 0.14
all heavy atoms	1.54 ± 0.19
MolProbity analysis[e]	
Clash score	94.39 ± 9.94
MolProbity score	4.37 ± 0.08

[a]None of these 20 structures exhibited distance violations of >0.2 Å or dihedral angle violations of >2°. [b]The number of each experimental constraint used in the calculations is given in parentheses. [c]F_{NOE}, F_{tor}, and F_{repel} are the energies related to the NOE violations, the torsion angle violations, and the van der Waals repulsion term, respectively. The values of the force constants used for these terms are the standard values as depicted in the X-PLOR 3.1 manual. $E_{L\text{-}J}$ is the Lennard-Jones van der Waals energy calculated with the CHARMm empirical energy function.[102] $E_{L\text{-}J}$ was not used in the dynamical simulated annealing calculations. [d]PROCHECK_NMR was used to assess the stereochemical quality of the structures. [e]The MolProbity webserver was used to evaluate the determined kurtoxin ensemble structures.

dx.doi.org/10.1021/bi201633j | Biochemistry 2012, 51, 1862–1873

kurtoxin. Several charged residues, including Asp[3], Lys[21], and Lys[56], surround the major surface hydrophobic patch, while Lys[13], Arg[14], and Asp[25] are situated near the minor hydrophobic patch (Figure 4D).

Structural Comparison of Kurtoxin with Scorpion α-Toxins. The amino acid sequence of kurtoxin is homologous with those of the scorpion α-toxins targeting Na^+ channels (Figure 1), which is consistent with the finding that kurtoxin can also interact with voltage-gated Na^+ channels.[55] The three-dimensional structures of the scorpion α-toxins have been determined by ^1H 2D NMR spectroscopy and X-ray crystallography.[91−101] Their overall folds are remarkably similar to that of kurtoxin and consist of an α-helix and three β-strands stabilized by four disulfide bridges, which has been termed the CSαβ (cysteine-stabilized α-helix and β-sheet) motif.[102] In addition, like kurtoxin, the α-helices of the scorpion α-toxins contain 2.5−3 helical turns and are connected to the central β-stand by two disulfide bridges.

Figure 5 shows the geometric average backbone structure from the 20 NMR kurtoxin models superimposed on the backbones of AaH II (antimammal α-toxin), LqhαIT (anti-insect α-toxin), and BmK M1 (α-like toxin). Comparison of the kurtoxin backbone with those of the scorpion α-toxins clearly highlights three regions of structural difference: the first long loop region (Asp[8]−Ile[15]), the β-hairpin loop (Gly[39]−Leu[42]), and the C-terminal segment (Arg[57]−Ala[63]). The structural differences among these regions are strongly correlated with a marked difference in sequence (Figure 1). Among the eight residues extending from Asp[8] to Ile[15], only two (Ans[11] and Cys[12]) are conserved in the amino acid sequences of these toxins. The 9th and 10th residues are variably polar or hydrophobic in the scorpion α-toxins, with a non-proline *cis* peptide bond in BMK M1.[99] On the other hand, they are bulky hydrophobic residues (Tyr[9] and Trp[10]) with a common *trans* peptide bond in kurtoxin. In addition, the structurally well-defined hydrophobic residues Val[13] and Tyr[14] found in LqhαIT and BmK M1 are replaced with disordered positively charged residues Lys[13] and Arg[14], respectively, in kurtoxin.

The sequence of the hairpin loop (Gly[39]−Leu[42]) also differs between kurtoxin and the scorpion α-toxins. The length of the loop in kurtoxin (four residues) is shorter than in other toxins (approximately seven residues). In addition, whereas the loop is disordered and involved in the formation of the major hydrophobic patch in kurtoxin, it protrudes from the CSαβ core and turns toward the C-terminal segments in the scorpion α-toxins (Figure 5). Because the C-terminal segments are disordered in both kurtoxin and scorpion α-toxins, it is difficult to assess structural differences in that region. However, site-directed mutagenesis studies and functional assays of scorpion α-toxins have shown that there is a functional site composed of the five-residue reverse turn (Asp[8]−Cys[12]) and the C-terminal segment, and that the conserved hydrophobic surface may be involved in maintaining the stability of the protein and its biological activity.[103−107] Taken together, these findings indicate that the core region of kurtoxin (i.e., the CSαβ motif) is well-defined and superimposes well on those of the scorpion α-toxins, but the Asp[8]−Ile[15], Gly[39]−Leu[42], and C-terminal segments of kurtoxin are structurally different from those of the scorpion α-toxins, suggesting it is these regions that are responsible for the functional differences between kurtoxin and scorpion α-toxins.

Comparison of the Surface Profiles of Kurtoxin and Scorpion α-Toxins. Kurtoxin contains five negatively charged and 11 positively charged residues in its amino acid sequence (Figure 1), and all of these charged residues except Asp[8] are highly exposed on the water-accessible surface of the molecule. The side chain oxygen of Asp[8] in AaH II forms a hydrogen bond with the amide proton of Val[10], and the side chain of Gln[8] in Lqh III forms a hydrogen bond with the oxygen of Val[13].[100] Asp[8] of kurtoxin is directed toward Lys[13] and Arg[14] (Figure 6A). Although there are no experimental data for the hydrogen bond interactions between Asp[8] and any other residues in kurtoxin, some side chain oxygens of Asp[8] in 20 ensemble structures are close enough to form hydrogen bonds with Lys[13] and/or Arg[14] in the determined kurtoxin structures. Along the α-helix, the positive and negative charges align toward the solvent-accessible region of the molecule in both scorpion α-toxins and kurtoxin (Figure 6), suggesting that this feature may be involved in ion channel binding and determining

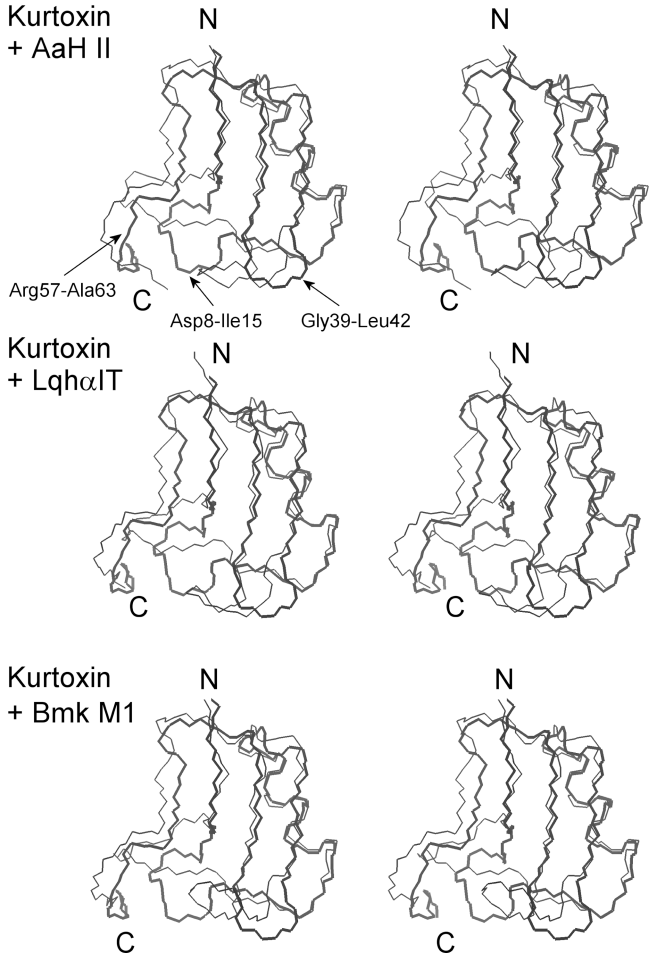

Figure 5. Stereopairs showing the superposition of the kurtoxin structure on scorpion α-toxin structures. The backbone (C, C^α, and N) atoms of kurtoxin are superimposed on those of the scorpion α-toxins. The top panel shows the superposition of the backbone of kurtoxin on that of the anti-mammal α-toxin AaH II (PDB entry 1PTX). The middle panel shows the superposition on the backbone of the anti-insect α-toxin LqhαIT (PDB entry 1LQH). The bottom panel shows the superposition on the backbone of the α-like toxin Bmk M1 (PDB entry 1DJT). The backbone structures of kurtoxin and scorpion α-toxins are shown as thick and thin lines, respectively. N and C indicate the N- and C-terminal positions, respectively. Labeling shows the kurtoxin residues in regions of structural difference between the two backbones. The backbone rmsd values are 3.13, 2.98, and 2.62 Å for AaH II, LqhαIT, and Bmk M1, respectively.

dx.doi.org/10.1021/bi201633j | *Biochemistry* 2012, 51, 1862−1873

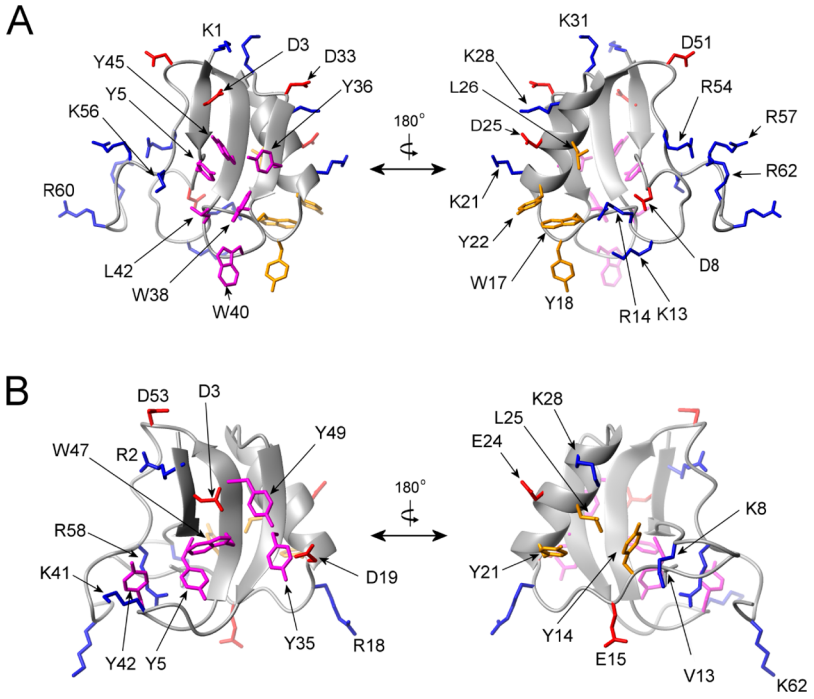

Figure 6. Ribbon diagrams and heavy atom side chains of kurtoxin (A) and Lqq III (B). The surface hydrophobic patches and charged residues are indicated: red for the negatively charged amino acids are colored, blue for the positively charged amino acids, purple for the major surface hydrophobic amino acids, and orange for the minor surface hydrophobic amino acids. The left and right figures are rotated 180° relative to one another about a vertical axis.

selectivity.[100] Kurtoxin is highly basic, as compared to the α-scorpion toxins; the net charge of kurtoxin is +6, while the others have net charges ranging from −2 to +3. As shown in Figure 1, the two hydrophobic residues (Val^{13} and Tyr^{14}) conserved in all scorpion α-toxins except AaH II are replaced with two positively charged residues (Lys^{13} and Arg^{14}, respectively) in kurtoxin. Figure 6B shows that the side chains of Val^{13} and Tyr^{14} in Lqq III (an anti-insect α-toxin) are largely buried in the molecular core. By contrast, Lys^{13} and Arg^{14} in kurtoxin are exposed to solvent (Figure 6A) and form a local electropositive surface (Figure 4D). In addition, a large electropositive patch (surface area of 660 Å^2) is formed by the five positively charged C-terminal residues (Arg^{54}, Lys^{56}, Arg^{57}, Arg^{60}, and Arg^{62}). This is in contrast to the C-terminal structure of Lqq III, which contains only two positively charged residues (Arg^{58} and Lys^{62}). The water-exposed, positively charged residues of kurtoxin form a distinctive large electropositive surface, which is located around the five-residue reverse turn and C-terminal segment and is the proposed Na^+ channel binding site in scorpion α-toxins.[104]

A surface hydrophobic patch is a conserved feature of all scorpion α-toxins and is involved in mediating their interaction with Na^+ channels.[108,109] The orthogonal arrangement of the aromatic side chains in the surface hydrophobic patch, termed a "herringbone" structure, is found in all scorpion α-toxins and has been identified as the lowest-energy configuration of solvent-exposed aromatic rings.[110] There are two hydrophobic patches in scorpion α-toxins, a major patch commonly composed of five residues (Tyr^5, Tyr^{35}, Tyr^{42}, Trp^{47}, and Tyr^{49}) (Figure 6B) with a surface area of ~280 Å^2 and a minor one with a surface area of ~210 Å^2. Kurtoxin exhibits a larger hydrophobic surface than the scorpion α-toxins. The major hydrophobic patch of kurtoxin consists of the six solvent-exposed side chains of Tyr^5, Tyr^{36}, Trp^{38}, Trp^{40}, Leu^{42}, and Tyr^{45} and has a surface area of 600 Å^2 (Figure 6A). The side chains are well-packed on each other, creating a compact hydrophobic patch on the protein surface. The minor hydrophobic patch (surface area of 500 Å^2) is centered on Trp^{17}, Tyr^{18}, and Tyr^{22} and also includes the δ-methyls of Leu^{26} (Figure 6A). Overall, it appears that kurtoxin shows a distinct surface profile, composed of both positive and hydrophobic residues, compared to other scorpion α-toxins.

Kurtoxin Binding Site on Cav3 (T-type) Ca^{2+} Channels. Voltage-gated ion channels consist of a central ion conduction pore (segments S5 and S6) surrounded by voltage sensors (segments S1−S4), which form "voltage sensor paddles" that move in response to changes in membrane voltage.[4,43] The overall structure of the voltage sensor paddles includes hydrophobic, cationic, and helix−turn−helix structures formed by the S3b−S4 segment, and it has been suggested that it is the voltage sensor paddles that are recognized by gating modifier toxins.[17−19,38−40,42,45] Kurtoxin has been identified as the first high-affinity (K_d = 15 nM) gating modifier of Cav3.1 (α1G T-type) Ca^{2+} channels, and also the first to show cross-reactivity with voltage-gated Na^+ channels.[55] This is similar to HaTx and GrTx, which exhibit cross-reactivity with the Kv2.1 K^+ channel and P/Q-type Ca^{2+} channel, modifying the energetics of their gating.[38] It has been suggested that hydrophobic and negatively charged residues (Ile^{273}, Phe^{274}, and Glu^{277}) in the Kv2.1 channel form the binding site for HaTx and GrTx.[38,111] Glu^{1613} in the rat brain IIA Na^+ channel is equivalent to Glu^{277} in the Kv2.1 channel, and mutation of Glu^{1613} has a large effect on the affinity of scorpion α-toxins for Na^+ channels.[17] In addition, Glu^{1658}, situated at the end of S3, within repeat IV of the P/Q-type Ca^{2+} channel, contributes to the binding of ω-Aga IVA.[19] These findings prompt us to speculate that kurtoxin may bind to the S3b−S4 motif in domain IV of both Cav3 (T-type) Ca^{2+} channels and Na^+ channels, a region that has some conservation

dx.doi.org/10.1021/bi201633j | Biochemistry 2012, 51, 1862−1873

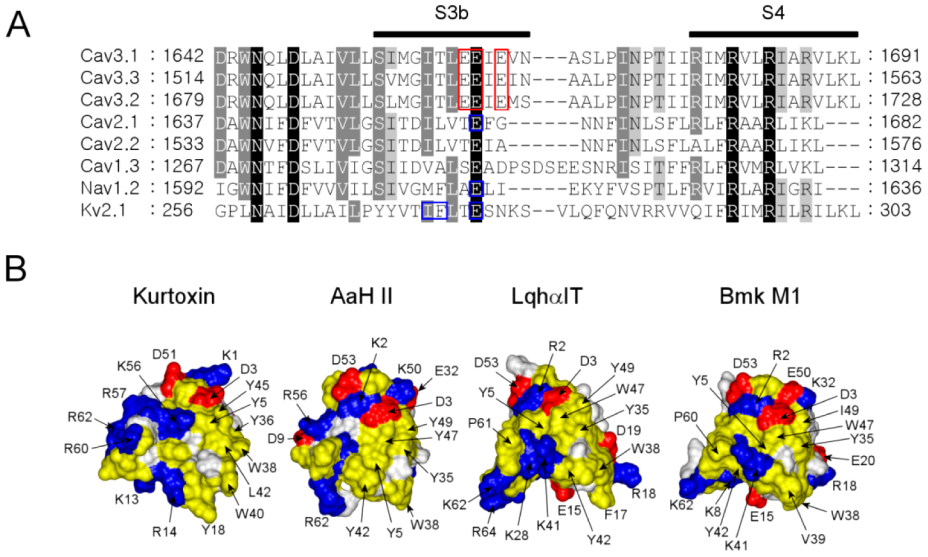

Figure 7. Comparison of the amino acid sequences of the indicated voltage-gated ion channels and the surface profiles of kurtoxin and scorpion α-toxins. (A) Comparison of the amino acid sequences of the domain IV S3−S4 linker in different voltage-gated ion channels (Cav, voltage-gated calcium channels; Nav, voltage-gated sodium channels; and Kv2.1, voltage-gated potassium channels). These sequences were aligned using ClustalX. Highly conserved residues are shaded in black or gray. The red rectangular boxes highlight the proposed kurtoxin binding site on Cav3 (T-type) Ca^{2+} channels. The blue rectangular boxes highlight the sequence involved in the binding sites of gating modifiers (Ile^{273}, Phe^{274}, and Glu^{277} in K^+ channels; Glu^{1613} in Na^+ channels; and Glu^{1658} in P/Q-type Ca^{2+} channels). (B) Surface profiles of kurtoxin, AaH II, LqqhαIT, and Bmk M1: yellow for hydrophobic residues (Ala, Cys, Gly, Leu, Ile, Phe, Pro, Trp, Tyr and Val), blue and red for basic (Arg and Lys) and acidic (Asp and Glu) residues, respectively, and white for other residues. The surface hydrophobic patch residues and charged residues are indicated.

between the two channels and that corresponds to the HaTx/GrTx binding site on voltage-gated K^+ and Ca^{2+} channels.[55] The region conserved in Cav3 (T-type) Ca^{2+} channels contains three glutamate residues [Glu^{1661}, Glu^{1662}, and Glu^{1664} for Cav3.1 (Figure 7A)]. Notably, the region in the Cav3 (T-type) Ca^{2+} channel makes a larger negative patch than in Na^+, K^+, or other types of Ca^{2+} channels, and this negative domain is conserved in all Cav3 (T-type) Ca^{2+} channel subtypes. As mentioned, kurtoxin is highly electropositive because of the presence of an electropositive patch formed by Lys^{13}, Arg^{14}, and five positively charged residues in the C-terminal segment (Arg^{54}, Lys^{56}, Arg^{57}, Arg^{60}, and Arg^{62}). We therefore speculate that the positively charged surface of kurtoxin is an important determinant of its binding to the conserved negative domain in Cav3 (T-type) Ca^{2+} channels. Figure 7B shows a comparison of the surface profiles of kurtoxin and three scorpion α-toxins. Kurtoxin exhibits surface characteristics arising from a surface hydrophobic patch in combination with a large electropositive patch. By contrast, scorpion α-toxins show a rather small surface hydrophobic patch with a mixed charged surface. These distinct surface profiles may explain why only kurtoxin is able to interact with the binding domain on Cav3 (T-type) Ca^{2+} channels, which is composed of electronegative and hydrophobic residues. We are currently in the process of preparing alanine mutants of kurtoxin and the Cav3.1 channel to examine the molecular basis of the interaction between the toxin and channel.

CONCLUSION

We investigated the three-dimensional structure of the first peptide toxin known to inhibit Cav3 (T-type) voltage-gated Ca^{2+} channels and suggest that its unique surface properties are likely responsible for its binding selectivity. Interestingly, kurtoxin can interact with high affinity with native neuronal high-threshold L-type, N-type, and P-type Ca^{2+} channels in central and peripheral neurons, producing complex gating modifications specific to each channel type.[56] When the channels are expressed in *Xenopus* oocytes, however, kurtoxin interacts only with the α-subunit of Cav3.1 (α1G T-type) voltage-gated Ca^{2+} channels; it does not interact with any other type of Ca^{2+} channel.[55] At present, the mechanism by which kurtoxin interacts with Ca^{2+} channels remains unknown. The structural studies of kurtoxin reported here provide clues about the molecular mechanism by which Cav3 (T-type) Ca^{2+} channel activity is regulated by selective ligands and could contribute to the development of highly specific Cav3 (T-type) Ca^{2+} channel inhibitors.

ASSOCIATED CONTENT

Supporting Information

Figures S1−S3. This material is available free of charge via the Internet at http://pubs.acs.org.

Accession Codes

The coordinates for kurtoxin have been deposited in the Protein Data Bank as entry 1T1T.

AUTHOR INFORMATION

Corresponding Author

*Department of Life Science, Gwangju Institute of Science and Technology (GIST), Gwangju 500-712, Republic of Korea. E-mail: jikim@gist.ac.kr. Telephone: +82-62-715-2494. Fax: +82-62-715-2484.

Funding

This research was supported by grants from the Next-Generation BioGreen 21 Program (PJ008158); the Rural Development Administration, Republic of Korea; a National Research Foundation of Korea grant funded by the Korean Government (MEST) (NRF-C1ABA001-2011-0018559); the Brain Research Center of the 21st Century Frontier Research

Program (M103KV010005-06K2201-00610); and the BioImaging Research Center at the Gwangju Institute of Science and Technology and Basic Research Projects in High-tech Industrial Technology funded by the Gwangju Institute of Science and Technology in 2011.

Notes

The authors declare no competing financial interest.

■ ACKNOWLEDGMENTS

We are grateful to Dr. Chul-Seung Park for critical reading of the manuscript.

■ ABBREVIATIONS

CD, circular dichroism; DSS, 4,4-dimethyl-4-silapentane-1-sulfonic acid; DQF-COSY, double-quantum-filtered correlation spectroscopy; E-COSY, exclusive COSY; HSQC, heteronuclear single-quantum coherence; MALDI-TOF MS, matrix-assisted laser desorption ionization time-of-flight mass spectrometry; NMR, nuclear magnetic resonance; NOE, nuclear Overhauser effect; NOESY, nuclear Overhauser effect spectroscopy; PDB, Protein Data Bank; RP-HPLC, reverse phase high-performance liquid chromatography; TOCSY, total correlated spectroscopy.

■ REFERENCES

(1) Doyle, D. A., Morais Cabral, J., Pfuetzner, R. A., Kuo, A., Gulbis, J. M., Cohen, S. L., Chait, B. T., and MacKinnon, R. (1998) The structure of the potassium channel: Molecular basis of K^+ conduction and selectivity. *Science 280*, 69−77.

(2) Kubo, Y., Baldwin, T. J., Jan, Y. N., and Jan, L. Y. (1993) Primary structure and functional expression of a mouse inward rectifier potassium channel. *Nature 362*, 127−133.

(3) Lu, Z., Klem, A. M., and Ramu, Y. (2001) Ion conduction pore is conserved among potassium channels. *Nature 413*, 809−813.

(4) Jiang, Y., Lee, A., Chen, J., Ruta, V., Cadene, M., Chait, B. T., and MacKinnon, R. (2003) X-ray structure of a voltage-dependent K^+ channel. *Nature 423*, 33−41.

(5) Possani, L. D., Merino, E., Corona, M., Bolivar, F., and Becerril, B. (2000) Peptides and genes coding for scorpion toxins that affect ion-channels. *Biochimie 82*, 861−868.

(6) Rash, L. D., and Hodgson, W. C. (2002) Pharmacology and biochemistry of spider venoms. *Toxicon 40*, 225−254.

(7) Terlau, H., and Olivera, B. M. (2004) Conus venoms: A rich source of novel ion channel-targeted peptides. *Physiol. Rev. 84*, 41−68.

(8) Norton, R. S., and McDonough, S. I. (2008) Peptides targeting voltage-gated calcium channels. *Curr. Pharm. Des. 14*, 2480−2491.

(9) French, R. J., and Dudley, S. C. Jr. (1999) Pore-blocking toxins as probes of voltage-dependent channels. *Methods Enzymol. 294*, 575−605.

(10) Bontems, F., Roumestand, C., Gilquin, B., Menez, A., and Toma, F. (1991) Refined structure of charybdotoxin: Common motifs in scorpion toxins and insect defensins. *Science 254*, 1521−1523.

(11) Davis, J. H., Bradley, E. K., Miljanich, G. P., Nadasdi, L., Ramachandran, J., and Basus, V. J. (1993) Solution structure of ω-conotoxin GVIA using 2-D NMR spectroscopy and relaxation matrix analysis. *Biochemistry 32*, 7396−7405.

(12) Farr-Jones, S., Miljanich, G. P., Nadasdi, L., Ramachandran, J., and Basus, V. J. (1995) Solution structure of ω-conotoxin MVIIC, a high affinity ligand of P-type calcium channels, using ^{1}H NMR spectroscopy and complete relaxation matrix analysis. *J. Mol. Biol. 248*, 106−124.

(13) Hill, J. M., Alewood, P. F., and Craik, D. J. (1996) Three-dimensional solution structure of mu-conotoxin GIIIB, a specific blocker of skeletal muscle sodium channels. *Biochemistry 35*, 8824−8835.

(14) Kohno, T., Kim, J. I., Kobayashi, K., Kodera, Y., Maeda, T., and Sato, K. (1995) Three-dimensional structure in solution of the calcium channel blocker ω-conotoxin MVIIA. *Biochemistry 34*, 10256−10265.

(15) Ott, K. H., Becker, S., Gordon, R. D., and Ruterjans, H. (1991) Solution structure of μ-conotoxin GIIIA analysed by 2D-NMR and distance geometry calculations. *FEBS Lett. 278*, 160−166.

(16) Li-Smerin, Y., and Swartz, K. J. (2000) Localization and molecular determinants of the Hanatoxin receptors on the voltage-sensing domains of a K^+ channel. *J. Gen. Physiol. 115*, 673−684.

(17) Rogers, J. C., Qu, Y., Tanada, T. N., Scheuer, T., and Catterall, W. A. (1996) Molecular determinants of high affinity binding of α-scorpion toxin and sea anemone toxin in the S3-S4 extracellular loop in domain IV of the Na^+ channel α subunit. *J. Biol. Chem. 271*, 15950−15962.

(18) Swartz, K. J., and MacKinnon, R. (1997) Hanatoxin modifies the gating of a voltage-dependent K^+ channel through multiple binding sites. *Neuron 18*, 665−673.

(19) Winterfield, J. R., and Swartz, K. J. (2000) A hot spot for the interaction of gating modifier toxins with voltage-dependent ion channels. *J. Gen. Physiol. 116*, 637−644.

(20) Catterall, W. A., Cestele, S., Yarov-Yarovoy, V., Yu, F. H., Konoki, K., and Scheuer, T. (2007) Voltage-gated ion channels and gating modifier toxins. *Toxicon 49*, 124−141.

(21) McDonough, S. I. (2007) Gating modifier toxins of voltage-gated calcium channels. *Toxicon 49*, 202−212.

(22) Cahalan, M. D. (1975) Modification of sodium channel gating in frog myelinated nerve fibres by *Centruroides sculpturatus* scorpion venom. *J. Physiol. 244*, 511−534.

(23) Cestele, S., Ben Khalifa, R. B., Pelhate, M., Rochat, H., and Gordon, D. (1995) α-Scorpion toxins binding on rat brain and insect sodium channels reveal divergent allosteric modulations by brevetoxin and veratridine. *J. Biol. Chem. 270*, 15153−15161.

(24) Fainzilber, M., Kofman, O., Zlotkin, E., and Gordon, D. (1994) A new neurotoxin receptor site on sodium channels is identified by a conotoxin that affects sodium channel inactivation in molluscs and acts as an antagonist in rat brain. *J. Biol. Chem. 269*, 2574−2580.

(25) Meves, H., Simard, J. M., and Watt, D. D. (1986) Interactions of scorpion toxins with the sodium channel. *Ann. N.Y. Acad. Sci. 479*, 113−132.

(26) Norton, R. S. (1991) Structure and structure-function relationships of sea anemone proteins that interact with the sodium channel. *Toxicon 29*, 1051−1084.

(27) Shon, K. J., Hasson, A., Spira, M. E., Cruz, L. J., Gray, W. R., and Olivera, B. M. (1994) δ-Conotoxin GmVIA, a novel peptide from the venom of *Conus gloriamaris*. *Biochemistry 33*, 11420−11425.

(28) Strichartz, G. R., and Wang, G. K. (1986) Rapid voltage-dependent dissociation of scorpion α-toxins coupled to Na channel inactivation in amphibian myelinated nerves. *J. Gen. Physiol. 88*, 413−435.

(29) Marvin, L., De, E., Cosette, P., Gagnon, J., Molle, G., and Lange, C. (1999) Isolation, amino acid sequence and functional assays of SGTx1. The first toxin purified from the venom of the spider scodra griseipes. *Eur. J. Biochem. 265*, 572−579.

(30) Ruta, V., Jiang, Y., Lee, A., Chen, J., and MacKinnon, R. (2003) Functional analysis of an archaebacterial voltage-dependent K^+ channel. *Nature 422*, 180−185.

(31) Swartz, K. J., and MacKinnon, R. (1995) An inhibitor of the Kv2.1 potassium channel isolated from the venom of a Chilean tarantula. *Neuron 15*, 941−949.

(32) Herrington, J. (2007) Gating modifier peptides as probes of pancreatic β-cell physiology. *Toxicon 49*, 231−238.

(33) Herrington, J., Zhou, Y. P., Bugianesi, R. M., Dulski, P. M., Feng, Y., Warren, V. A., Smith, M. M., Kohler, M. G., Garsky, V. M., Sanchez, M., Wagner, M., Raphaelli, K., Banerjee, P., Ahaghotu, C., Wunderler, D., Priest, B. T., Mehl, J. T., Garcia, M. L., McManus, O. B., Kaczorowski, G. J., and Slaughter, R. S. (2006) Blockers of the delayed-rectifier potassium current in pancreatic β-cells enhance glucose-dependent insulin secretion. *Diabetes 55*, 1034−1042.

(34) Lampe, R. A., Defeo, P. A., Davison, M. D., Young, J., Herman, J. L., Spreen, R. C., Horn, M. B., Mangano, T. J., and Keith, R. A. (1993) Isolation and pharmacological characterization of ω-grammotoxin SIA, a novel peptide inhibitor of neuronal voltage-sensitive calcium channel responses. *Mol. Pharmacol. 44*, 451−460.
(35) McDonough, S. I., Lampe, R. A., Keith, R. A., and Bean, B. P. (1997) Voltage-dependent inhibition of N- and P-type calcium channels by the peptide toxin ω-grammotoxin-SIA. *Mol. Pharmacol. 52*, 1095−1104.
(36) Mintz, I. M., Adams, M. E., and Bean, B. P. (1992) P-type calcium channels in rat central and peripheral neurons. *Neuron 9*, 85−95.
(37) Mintz, I. M., Venema, V. J., Swiderek, K. M., Lee, T. D., Bean, B. P., and Adams, M. E. (1992) P-type calcium channels blocked by the spider toxin ω-Aga-IVA. *Nature 355*, 827−829.
(38) Li-Smerin, Y., and Swartz, K. J. (1998) Gating modifier toxins reveal a conserved structural motif in voltage-gated Ca^{2+} and K^+ channels. *Proc. Natl. Acad. Sci. U.S.A. 95*, 8585−8589.
(39) Wang, J. M., Roh, S. H., Kim, S., Lee, C. W., Kim, J. I., and Swartz, K. J. (2004) Molecular surface of tarantula toxins interacting with voltage sensors in K(v) channels. *J. Gen. Physiol. 123*, 455−467.
(40) Swartz, K. J. (2007) Tarantula toxins interacting with voltage sensors in potassium channels. *Toxicon 49*, 213−230.
(41) Milescu, M., Bosmans, F., Lee, S., Alabi, A. A., Kim, J. I., and Swartz, K. J. (2009) Interactions between lipids and voltage sensor paddles detected with tarantula toxins. *Nat. Struct. Mol. Biol. 16*, 1080−1085.
(42) Alabi, A. A., Bahamonde, M. I., Jung, H. J., Kim, J. I., and Swartz, K. J. (2007) Portability of paddle motif function and pharmacology in voltage sensors. *Nature 450*, 370−375.
(43) Jiang, Y., Ruta, V., Chen, J., Lee, A., and MacKinnon, R. (2003) The principle of gating charge movement in a voltage-dependent K^+ channel. *Nature 423*, 42−48.
(44) Long, S. B., Tao, X., Campbell, E. B., and MacKinnon, R. (2007) Atomic structure of a voltage-dependent K^+ channel in a lipid membrane-like environment. *Nature 450*, 376−382.
(45) Milescu, M., Vobecky, J., Roh, S. H., Kim, S. H., Jung, H. J., Kim, J. I., and Swartz, K. J. (2007) Tarantula toxins interact with voltage sensors within lipid membranes. *J. Gen. Physiol. 130*, 497−511.
(46) Perez-Reyes, E. (2003) Molecular physiology of low-voltage-activated t-type calcium channels. *Physiol. Rev. 83*, 117−161.
(47) Chen, C. F., Corbley, M. J., Roberts, T. M., and Hess, P. (1988) Voltage-sensitive calcium channels in normal and transformed 3T3 fibroblasts. *Science 239*, 1024−1026.
(48) Cohen, C. J., McCarthy, R. T., Barrett, P. Q., and Rasmussen, H. (1988) Ca channels in adrenal glomerulosa cells: K^+ and angiotensin II increase T-type Ca channel current. *Proc. Natl. Acad. Sci. U.S.A. 85*, 2412−2416.
(49) Huguenard, J. R. (1996) Low-threshold calcium currents in central nervous system neurons. *Annu. Rev. Physiol. 58*, 329−348.
(50) Steriade, M., and Llinas, R. R. (1988) The functional states of the thalamus and the associated neuronal interplay. *Physiol. Rev. 68*, 649−742.
(51) Iftinca, M. C., and Zamponi, G. W. (2009) Regulation of neuronal T-type calcium channels. *Trends Pharmacol. Sci. 30*, 32−40.
(52) Nelson, M. T., Todorovic, S. M., and Perez-Reyes, E. (2006) The role of T-type calcium channels in epilepsy and pain. *Curr. Pharm. Des. 12*, 2189−2197.
(53) Lory, P., and Chemin, J. (2007) Towards the discovery of novel T-type calcium channel blockers. *Expert Opin. Ther. Targets 11*, 717−722.
(54) Heady, T. N., Gomora, J. C., Macdonald, T. L., and Perez-Reyes, E. (2001) Molecular pharmacology of T-type Ca^{2+} channels. *Jpn. J. Pharmacol. 85*, 339−350.
(55) Chuang, R. S., Jaffe, H., Cribbs, L., Perez-Reyes, E., and Swartz, K. J. (1998) Inhibition of T-type voltage-gated calcium channels by a new scorpion toxin. *Nat. Neurosci. 1*, 668−674.
(56) Sidach, S. S., and Mintz, I. M. (2002) Kurtoxin, a gating modifier of neuronal high- and low-threshold ca channels. *J. Neurosci. 22*, 2023−2034.
(57) Lee, C. W., Kim, S., Roh, S. H., Endoh, H., Kodera, Y., Maeda, T., Kohno, T., Wang, J. M., Swartz, K. J., and Kim, J. I. (2004) Solution structure and functional characterization of SGTx1, a modifier of Kv2.1 channel gating. *Biochemistry 43*, 890−897.
(58) Takahashi, H., Kim, J. I., Min, H. J., Sato, K., Swartz, K. J., and Shimada, I. (2000) Solution structure of hanatoxin1, a gating modifier of voltage-dependent K^+ channels: Common surface features of gating modifier toxins. *J. Mol. Biol. 297*, 771−780.
(59) Lee, C. W., Eu, Y. J., Min, H. J., Cho, E. M., Lee, J. H., Kim, H. H., Nah, S. Y., Swartz, K. J., and Kim, J. I. (2011) Expression and characterization of recombinant kurtoxin, an inhibitor of T-type voltage-gated calcium channels. *Biochem. Biophys. Res. Commun. 416*, 277−282.
(60) Bax, A., and Davis, D. G. (1985) MLEV-17-based two-dimensional homonuclear magnetization transfer spectroscopy. *J. Magn. Reson. 65*, 355−360.
(61) Jeener, J., Meier, B. H., Bachmann, P., and Ernst, R. R. (1979) Investigation of exchange processes by two-dimensional NMR spectroscopy. *J. Chem. Phys. 71*, 4546−4553.
(62) Macura, S., Huang, Y., Suter, D., and Ernst, R. R. (1981) Two-Dimensional Chemical Exchange and Cross-Relaxation Spectroscopy of Coupled Nuclear Spins. *J. Magn. Reson. 43*, 259−281.
(63) Piotto, M., Saudek, V., and Sklenar, V. (1992) Gradient-tailored excitation for single-quantum NMR spectroscopy of aqueous solutions. *J. Biomol. NMR 2*, 661−665.
(64) Griesinger, C., Sørensen, O. W., and Ernst, R. R. (1987) Practical Aspects of the E-Cosy Technique: Measurement of Scalar Spin Spin Coupling-Constants in Peptides. *J. Magn. Reson. 75*, 474−492.
(65) Grzesiek, S., and Bax, A. (1992) Correlating backbone amide and side chain resonances in larger proteins by multiple relayed triple resonance NMR. *J. Am. Chem. Soc. 114*, 6291−6293.
(66) Kay, L. E., Ikura, M., Tschudin, R., and Bax, A. (1990) Three-dimensional triple-resonance NMR spectroscopy of isotopically enriched proteins. *J. Magn. Reson. 89*, 496−514.
(67) Muhandiram, D. R., and Kay, L. E. (1994) Gradient-enhanced triple-resonance three-dimensional NMR experiments with improved sensitivity. *J. Magn. Reson., Ser. B 103*, 203−216.
(68) Wittekind, M., and Mueller, L. (1993) HNCACB, a high-sensititity 3D NMR experiment to correlate amide-proton and nitrogen resonances with the α- and β-carbon resonaces in proteins. *J. Magn. Reson. 101*, 201−205.
(69) Bodenhausen, G., and Ruben, D. J. (1980) Natural abundance nitrogen-15 NMR by enhanced heteronuclear spectroscopy. *Chem. Phys. Lett. 69*, 185−189.
(70) Vuister, G. W., and Bax, A. (1993) Quantitative J Correlation: A New Approach for Measuring Homonuclear 3-Bond J(H(N)H(α) Coupling-Constants in N-15-Enriched Proteins. *J. Am. Chem. Soc. 115*, 7772−7777.
(71) Kraulis, P. J., Domaille, P. J., Campbell-Burk, S. L., Van Aken, T., and Laue, E. D. (1994) Solution structure and dynamics of ras p21.GDP determined by heteronuclear three- and four-dimensional NMR spectroscopy. *Biochemistry 33*, 3515−3531.
(72) Kline, A. D., Braun, W., and Wuthrich, K. (1988) Determination of the complete three-dimensional structure of the α-amylase inhibitor Tendamistat in aqueous solution by nuclear magnetic resonance and distance geometry. *J. Mol. Biol. 204*, 675−724.
(73) Pardi, A., Billeter, M., and Wuthrich, K. (1984) Calibration of the angular dependence of the amide proton-C α proton coupling constants, $^3J_{HN\alpha}$, in a globular protein. Use of $^3J_{HN\alpha}$ for identification of helical secondary structure. *J. Mol. Biol. 180*, 741−751.
(74) Hyberts, S. G., Marki, W., and Wagner, G. (1987) Stereospecific assignments of side-chain protons and characterization of torsion angles in Eglin c. *Eur. J. Biochem. 164*, 625−635.
(75) Wagner, G., Braun, W., Havel, T. F., Schaumann, T., Go, N., and Wuthrich, K. (1987) Protein structures in solution by nuclear

magnetic resonance and distance geometry. The polypeptide fold of the basic pancreatic trypsin inhibitor determined using two different algorithms, DISGEO and DISMAN. *J. Mol. Biol. 196*, 611−639.
(76) Wuthrich, K., Billeter, M., and Braun, W. (1983) Pseudo-structures for the 20 common amino acids for use in studies of protein conformations by measurements of intramolecular proton-proton distance constraints with nuclear magnetic resonance. *J. Mol. Biol. 169*, 949−961.
(77) Clore, G. M., Gronenborn, A. M., Nilges, M., and Ryan, C. A. (1987) Three-dimensional structure of potato carboxypeptidase inhibitor in solution. A study using nuclear magnetic resonance, distance geometry, and restrained molecular dynamics. *Biochemistry 26*, 8012−8023.
(78) Nilges, M., Gronenborn, A. M., Brunger, A. T., and Clore, G. M. (1988) Determination of three-dimensional structures of proteins by simulated annealing with interproton distance restraints. Application to crambin, potato carboxypeptidase inhibitor and barley serine proteinase inhibitor 2. *Protein Eng. 2*, 27−38.
(79) Fletcher, J. I., Chapman, B. E., Mackay, J. P., Howden, M. E., and King, G. F. (1997) The structure of versutoxin (δ-atracotoxin-Hv1) provides insights into the binding of site 3 neurotoxins to the voltage-gated sodium channel. *Structure 5*, 1525−1535.
(80) Fletcher, J. I., Smith, R., O'Donoghue, S. I., Nilges, M., Connor, M., Howden, M. E., Christie, M. J., and King, G. F. (1997) The structure of a novel insecticidal neurotoxin, ω-atracotoxin-HV1, from the venom of an Australian funnel web spider. *Nat. Struct. Biol. 4*, 559−566.
(81) Brunger, A. T. (1992) *X-PLOR Manual*, version 3.1, Yale University, New Haven, CT.
(82) Laskowski, R. A., Rullmannn, J. A., MacArthur, M. W., Kaptein, R., and Thornton, J. M. (1996) AQUA and PROCHECK-NMR: Programs for checking the quality of protein structures solved by NMR. *J. Biomol. NMR 8*, 477−486.
(83) Hutchinson, E. G., and Thornton, J. M. (1996) PROMOTIF: A program to identify and analyze structural motifs in proteins. *Protein Sci. 5*, 212−220.
(84) Koradi, R., Billeter, M., and Wuthrich, K. (1996) MOLMOL: A program for display and analysis of macromolecular structures. *J. Mol. Graphics 14*, 51−55 , 29−32.
(85) Chen, V. B., Arendall, W. B. III, Headd, J. J., Keedy, D. A., Immormino, R. M., Kapral, G. J., Murray, L. W., Richardson, J. S., and Richardson, D. C. (2010) MolProbity: All-atom structure validation for macromolecular crystallography. *Acta Crystallogr. D66*, 12−21.
(86) Davis, I. W., Leaver-Fay, A., Chen, V. B., Block, J. N., Kapral, G. J., Wang, X., Murray, L. W., Arendall, W. B. III, Snoeyink, J., Richardson, J. S., and Richardson, D. C. (2007) MolProbity: All-atom contacts and structure validation for proteins and nucleic acids. *Nucleic Acids Res. 35*, W375−W383.
(87) Hyberts, S. G., Goldberg, M. S., Havel, T. F., and Wagner, G. (1992) The solution structure of eglin c based on measurements of many NOEs and coupling constants and its comparison with X-ray structures. *Protein Sci. 1*, 736−751.
(88) Schmitke, J. L., Stern, L. J., and Klibanov, A. M. (1998) Comparison of X-ray crystal structures of an acyl-enzyme intermediate of subtilisin Carlsberg formed in anhydrous acetonitrile and in water. *Proc. Natl. Acad. Sci. U.S.A. 95*, 12918−12923.
(89) Morellet, N., Bouaziz, S., Petitjean, P., and Roques, B. P. (2003) NMR structure of the HIV-1 regulatory protein VPR. *J. Mol. Biol. 327*, 215−227.
(90) Zhu, J., Tong, X., Cao, C., Wu, G., Zhang, N., and Wu, H. (2010) Solution structure of BmKαTx11, a toxin from the venom of the Chinese scorpion *Buthus martensii* Karsch. *Biochem. Biophys. Res. Commun. 391*, 627−633.
(91) Zhao, B., Carson, M., Ealick, S. E., and Bugg, C. E. (1992) Structure of scorpion toxin variant-3 at 1.2 Å resolution. *J. Mol. Biol. 227*, 239−252.
(92) Housset, D., Habersetzer-Rochat, C., Astier, J. P., and Fontecilla-Camps, J. C. (1994) Crystal structure of toxin II from the scorpion *Androctonus australis* Hector refined at 1.3 Å resolution. *J. Mol. Biol. 238*, 88−103.
(93) Lebreton, F., Delepierre, M., Ramirez, A. N., Balderas, C., and Possani, L. D. (1994) Primary and NMR three-dimensional structure determination of a novel crustacean toxin from the venom of the scorpion *Centruroides limpidus limpidus* Karsch. *Biochemistry 33*, 11135−11149.
(94) Lee, W., Moore, C. H., Watt, D. D., and Krishna, N. R. (1994) Solution structure of the variant-3 neurotoxin from *Centruroides sculpturatus* Ewing. *Eur. J. Biochem. 219*, 89−95.
(95) Jablonsky, M. J., Watt, D. D., and Krishna, N. R. (1995) Solution structure of an Old World-like neurotoxin from the venom of the New World scorpion *Centruroides sculpturatus* Ewing. *J. Mol. Biol. 248*, 449−458.
(96) Li, H. M., Wang, D. C., Zeng, Z. H., Jin, L., and Hu, R. Q. (1996) Crystal structure of an acidic neurotoxin from scorpion *Buthus martensii* Karsch at 1.85 Å resolution. *J. Mol. Biol. 261*, 415−431.
(97) Landon, C., Sodano, P., Cornet, B., Bonmatin, J. M., Kopeyan, C., Rochat, H., Vovelle, F., and Ptak, M. (1997) Refined solution structure of the anti-mammal and anti-insect LqqIII scorpion toxin: Comparison with other scorpion toxins. *Proteins 28*, 360−374.
(98) Tugarinov, V., Kustanovich, I., Zilberberg, N., Gurevitz, M., and Anglister, J. (1997) Solution structures of a highly insecticidal recombinant scorpion α-toxin and a mutant with increased activity. *Biochemistry 36*, 2414−2424.
(99) He, X. L., Li, H. M., Zeng, Z. H., Liu, X. Q., Wang, M., and Wang, D. C. (1999) Crystal structures of two α-like scorpion toxins: Non-proline cis peptide bonds and implications for new binding site selectivity on the sodium channel. *J. Mol. Biol. 292*, 125−135.
(100) Krimm, I., Gilles, N., Sautiere, P., Stankiewicz, M., Pelhate, M., Gordon, D., and Lancelin, J. M. (1999) NMR structures and activity of a novel α-like toxin from the scorpion *Leiurus quinquestriatus hebraeus*. *J. Mol. Biol. 285*, 1749−1763.
(101) Jablonsky, M. J., Jackson, P. L., and Krishna, N. R. (2001) Solution structure of an insect-specific neurotoxin from the New World scorpion *Centruroides sculpturatus* Ewing. *Biochemistry 40*, 8273−8282.
(102) Cornet, B., Bonmatin, J. M., Hetru, C., Hoffmann, J. A., Ptak, M., and Vovelle, F. (1995) Refined three-dimensional solution structure of insect defensin A. *Structure 3*, 435−448.
(103) Kahn, R., Karbat, I., Ilan, N., Cohen, L., Sokolov, S., Catterall, W. A., Gordon, D., and Gurevitz, M. (2009) Molecular Requirements for Recognition of Brain Voltage-gated Sodium Channels by Scorpion α-Toxins. *J. Biol. Chem. 284*, 20684−20691.
(104) Zilberberg, N., Froy, O., Loret, E., Cestele, S., Arad, D., Gordon, D., and Gurevitz, M. (1997) Identification of structural elements of a scorpion α-neurotoxin important for receptor site recognition. *J. Biol. Chem. 272*, 14810−14816.
(105) Sun, Y. M., Bosmans, F., Zhu, R. H., Goudet, C., Xiong, Y. M., Tytgat, J., and Wang, D. C. (2003) Importance of the conserved aromatic residues in the scorpion α-like toxin BmK M1: The hydrophobic surface region revisited. *J. Biol. Chem. 278*, 24125−24131.
(106) Wang, C. G., Gilles, N., Hamon, A., Le Gall, F., Stankiewicz, M., Pelhate, M., Xiong, Y. M., Wang, D. C., and Chi, C. W. (2003) Exploration of the functional site of a scorpion α-like toxin by site-directed mutagenesis. *Biochemistry 42*, 4699−4708.
(107) Ye, X., Bosmans, F., Li, C., Zhang, Y., Wang, D. C., and Tytgat, J. (2005) Structural basis for the voltage-gated Na^+ channel selectivity of the scorpion α-like toxin BmK M1. *J. Mol. Biol. 353*, 788−803.
(108) Fontecilla-Camps, J. C., Habersetzer-Rochat, C., and Rochat, H. (1988) Orthorhombic crystals and three-dimensional structure of the potent toxin II from the scorpion *Androctonus australis* Hector. *Proc. Natl. Acad. Sci. U.S.A. 85*, 7443−7447.
(109) Li, H. M., Zhao, T., Jin, L., Wang, M., Zhang, Y., and Wang, D. C. (1999) A series of bioactivity-variant neurotoxins from scorpion *Buthus martensii* Karsch: Purification, crystallization and crystallographic analysis. *Acta Crystallogr. D55*, 341−344.

(110) Burley, S. K., and Petsko, G. A. (1985) Aromatic-aromatic interaction: A mechanism of protein structure stabilization. *Science 229*, 23−28.
(111) Swartz, K. J., and MacKinnon, R. (1997) Mapping the receptor site for hanatoxin, a gating modifier of voltage-dependent K^+ channels. *Neuron 18*, 675−682.